

2017-06-01


## Industrial grade 2D Molybdenum Disulphide (MoS<sub>2</sub>): An in-vitro exploration of the impact on cellular uptake, cytotoxicity, and inflammation

Caroline Moore  
*Technological University Dublin*

Hugh Byrne  
*Technological University Dublin, [hugh.byrne@tudublin.ie](mailto:hugh.byrne@tudublin.ie)*

Jonathan N. Coleman  
*Trinity College Dublin*

Yuri Volkov  
*Trinity College, Dublin, Ireland*  
Follow this and additional works at: <https://arrow.tudublin.ie/biophonart>

 **Yvonne McIntyre**, Materials Chemistry Commons, Other Biochemistry, Biophysics, and Structural Biology Commons, Pharmacology, Toxicology and Environmental Health Commons, and the Physics Commons  
*Technological University Dublin*

### Recommended Citation

McIntyre, J. et al. (2017) Industrial grade 2D Molybdenum Disulphide (MoS<sub>2</sub>): An in-vitro exploration of the impact on cellular uptake, cytotoxicity, and inflammation", 2-D Materials, 4, 25065 (2017) DOI: 10.1088/2053-1583/aa673f

This Article is brought to you for free and open access by the DIT Biophotonics and Imaging at ARROW@TU Dublin. It has been accepted for inclusion in Articles by an authorized administrator of ARROW@TU Dublin. For more information, please contact [yvonne.desmond@tudublin.ie](mailto:yvonne.desmond@tudublin.ie), [arrow.admin@tudublin.ie](mailto:arrow.admin@tudublin.ie), [brian.widdis@tudublin.ie](mailto:brian.widdis@tudublin.ie).



This work is licensed under a [Creative Commons Attribution-Noncommercial-Share Alike 3.0 License](https://creativecommons.org/licenses/by-nc-sa/3.0/)

## **Industrial grade 2D Molybdenum Disulphide (MoS<sub>2</sub>): An *in-vitro* exploration of the impact on cellular uptake, cytotoxicity, and inflammation**

Caroline Moore<sup>1,2</sup>, Dania Movia<sup>2</sup>, Ronan J. Smith<sup>3</sup>, Damien Hanlon<sup>4</sup>, Filipa Lebre<sup>4,5</sup>, Ed C. Lavelle<sup>4,5</sup>, Hugh J. Byrne<sup>1</sup>, Jonathan N. Coleman<sup>4</sup>, Yuri Volkov<sup>2,4</sup>, Jennifer McIntyre<sup>1\*</sup>

1. FOCAS Research Institute, Dublin Institute of Technology, Ireland.
2. Department of Clinical Medicine, School of Medicine, Trinity College Dublin, Ireland.
3. School of Chemistry, Trinity College Dublin, Ireland.
4. Centre for Research on Adaptive Nanostructures & Nanodevices (CRANN) and Advanced Materials and BioEngineering Research (AMBER) Centre, Trinity College Dublin, Ireland.
5. Adjuvant Research Group, School of Biochemistry and Immunology, Trinity Biomedical Sciences Institute, Trinity College Dublin, Dublin 2, D02 PN40, Ireland.

\* Corresponding author email: [Jennifer.mcintyre@dit.ie](mailto:Jennifer.mcintyre@dit.ie)

## Abstract

The recent surge in graphene research, since its liquid phase monolayer isolation and characterization in 2004, has led to advancements which are accelerating the exploration of alternative 2D materials such as molybdenum disulphide ( $\text{MoS}_2$ ), whose unique physico-chemical properties can be exploited in applications ranging from cutting edge electronic devices to nanomedicine. However, to assess any potential impact on human health and the environment, the need to understand the bio-interaction of  $\text{MoS}_2$  at a cellular and sub-cellular level is critical. Notably, it is important to assess such potential impacts of materials which are produced by large scale production techniques, rather than research grade materials.

The aim of this study was to explore cytotoxicity, cellular uptake and inflammatory responses in established cell-lines that mimic different potential exposure routes (inhalation, A549; ingestion, AGS; monocyte, THP-1) following incubation with  $\text{MoS}_2$  flakes of varying sizes (50 nm, 117 nm and 177 nm), produced by liquid phase exfoliation. Using high content screening (HCS) and live/dead assays, it was established that 1  $\mu\text{g}/\text{ml}$  (for the three different  $\text{MoS}_2$  sizes) did not induce toxic effects on any of the cell-lines. Confocal microscopy images revealed a normal cellular morphology in all cases. Transmission electron microscopy (TEM) confirmed the uptake of all  $\text{MoS}_2$  nanomaterials in all the cell-lines, the  $\text{MoS}_2$  ultimately locating in single membrane vesicles. At such sub-lethal doses, inflammatory responses are observed, however, associated, at least partially, with the presence of lipopolysaccharide endotoxin in nanomaterial suspensions and surfactant samples. Therefore, the inflammatory response of the cells to the  $\text{MoS}_2$  or endotoxin contamination was interrogated using a 10-plex ELISA which illustrates cytokine production. The experiments carried out using wild-type and endotoxin hyporesponsive bone marrow derived dendritic cells confirmed that the inflammatory responses result from a combination of endotoxin contamination, the  $\text{MoS}_2$  nanomaterials themselves, and the stabilizing surfactant.

**Keywords:**  $\text{MoS}_2$ , 2D nanomaterials, cytotoxicity, uptake, endotoxin, inflammatory response

## Introduction

Over the past few decades, an increasing amount of research has been devoted to the field of nanotechnology, resulting in an ever increasing range of engineered nanoparticulate materials in both the research and consumer arenas. However, although exciting technological developments and nanomedical applications are emerging, it has become important to consider any potentially detrimental impacts of these materials on human health and the environment, giving rise to the field of nanotoxicology.

Nanomaterial classification is based on the number of dimensions that are not confined to the nanoscale range, generating four main categories; zero-dimensional (0D), one-dimensional (1D), two-dimensional (2D) and three-dimensional (3D) nanostructures (1). Nano-crystalline material is an example of a 3D nanostructure, which has been well characterised and studied, due to effective production of large scale quality crystals (2,3). Research in 2D materials, previously largely restricted to epitaxially grown semiconductor (multiple) quantum well structures, has exploded more recently since the demonstration of facile, large scale production of exfoliated graphene samples (3,4). Graphene has been extensively characterized due to its enhanced properties for applications such as semiconductors, bio-sensors and transparent electrodes for use in flexible devices, although the presence of a “zero band gap” has limited its applications for purposes of optoelectronics (5). Liquid based monolayer isolation and characterisation of graphene was reported in 2004, leading to the development of a wide spectrum of techniques for the synthesis, detection, characterisation and manipulation of 2D nanomaterials (6). The identification of these techniques has indeed allowed the acceleration of research on 2D materials other than graphene, such as boron nitride (BN) and molybdenum disulphide ( $\text{MoS}_2$ ), which was not possible prior to these new advancements.

$\text{MoS}_2$  is a 2D nanomaterial that is produced in plate-like particles formed by layers of chemically bonded atoms, which are stacked and held together by van der Waals interactions in the form of nanoplates or nanobelts (7).  $\text{MoS}_2$  has a low friction coefficient (0.003), allowing its use as a common lubricant, but it has shown great potential also as a transition metal dichalcogenides (TMDs) due to its enhanced indirect band gap of 1.9 eV when scaled down from bulk composites (8). It has been demonstrated that the “Coleman

method" of exfoliation (4) can also be applied to MoS<sub>2</sub>, yielding high quality dispersed sheets and allowing potentially scalable techniques to manufacture bulk quantities of MoS<sub>2</sub> nanosheets of controllable size (9,10) with potential applications in high performance electronics, semiconductors, light emitting and bio-sensor devices, and nanomedicine (11–13).

The foreseeable flexible transparent displays, enhanced energy storage systems or nanomedical applications can be made possible with large scale synthesis of 2D nanomaterials. However, before translation into industrial or biomedical arenas, the question of MoS<sub>2</sub> cytotoxicity, uptake and inflammatory response should be addressed to understand the potential health impacts following exposure during material synthesis, device manufacturing, consumer or patient exposure. For biomedical applications, the use of nanomaterials can increase drug delivery, reduce systemic effects and potentially cause confined detrimental effects to abnormal and/or cancerous cells using a targeted nanotherapy (14). Internalisation of nanomaterials can improve drug delivery while improving efficiency, as higher concentrations are delivered within each cell while healthy and/or neighbouring cells are protected. Therefore, extensive evaluation of 2D nanomaterial biosafety should be completed before translation into newly engineered technologically relevant devices and prior to commencement of clinical trials for drug delivery or gene silencing applications using MoS<sub>2</sub> nanomaterials (15,16). Unlike those 2D materials used for biomedical applications which are sterile and free of any contaminants, those produced on a large scale production for industrial applications are not produced to the same rigorous standards of purity.

Nanomaterial characterisation is therefore essential to predict and allow accurate determination of what cells are interacting with, where toxicity is originating, and the stability of newly synthesized nanomaterials. Nanoparticle size and surface charge play an important role when interacting with proteins present in biological fluids. Proteins and/or contaminants will actively bind to the nanomaterial surface potentially misdirecting the cells from identifying the nanomaterial, altering size and/or surface charge (17). A nanoparticle along with a protein corona can help by evading an immune response, improving the therapeutic efficacy of drugs or preventing nanomaterials reaching its final destination if the structure exceeds the size of biological barriers (18). Organs such as the liver and the spleen

are major contributors for the removal and secretion of nanomaterials following inhalation, oral ingestion or intravenous injection. Therefore determining an accurate nanomaterial size before exposure is essential to understand if nanomaterials will be rapidly excreted (<5µm), retained in specific organs or evenly distributed throughout the body (19). It has been shown that particles of larger sizes are most likely to be deposited in the upper airways while smaller sizes of nanomaterials can be transported to the alveolar region, increase toxicity and travel to secondary organs causing systemic effects (20,21). After inhalation and deposition in the lungs, this causes an influx of inflammatory cells as a protective mechanism in the presence of foreign material within the respiratory system. Infiltration of alveolar macrophages function by engulfing foreign materials and releasing inflammatory cytokines (22). Actively beating cilia along with mucus present in the lungs allows the upward movement of material which can be later swallowed. Gastrointestinal absorption is not the most common form of exposure, but given the increasing use of nanomaterial in sunscreens, cosmetics and food additives, there is increased risk to transfer nanomaterial residues by hand-to-mouth action (23,24).

Adverse effects to the respiratory tract, such as chronic inflammation and pulmonary fibrosis, are associated with exposure to many other ultra-fine nanomaterials produced by industry or present in air pollution. It is well known that such factors as nanomaterial size along with surface charge (25), aggregation and/or agglomeration play a crucial role in influencing immune response after human exposure. There has been an extensive amount of research carried out on the toxicity of 2D graphene and its derivatives, such as graphene oxide (GO) (26,27), amine-GO (28), carboxylated-GO (29) and graphene nanoribbons (30); in all cases the toxicity is dependent on the surface chemistry of the graphene (31). However, the toxicity and bio-interaction of MoS<sub>2</sub> are largely underexplored. Studies to date indicate that MoS<sub>2</sub> is less toxic than graphene and its analogues (32), but that the toxicity of MoS<sub>2</sub> increases with increasing degree of exfoliation (33). Therefore, with the increasing use and applications of MoS<sub>2</sub> nanomaterials at the present time, the potential health implications and basis of any toxicity should be investigated in depth prior to mass production. Depending on their application or environmental discharge route, nanomaterials can come into contact with the human body by inhalation, dermal contact, orally with subsequent absorption in the gastrointestinal tract or parenterally (34). If MoS<sub>2</sub> nanomaterials are to be

used for biomedical applications and drug delivery, confirming cellular uptake of nanosheets of varying sizes will play a crucial role in demonstrating whether effective drug delivery can be achieved, and if certain nanosheet sizes would influence the process. MoS<sub>2</sub> produced for enhanced electronic devices will involve potential exposure routes of nanomaterials at the manufacturing stage, consumer use or the end of their lifecycle after disposal (35). In this study, an extensive investigation of the cellular uptake, cytotoxicity and inflammatory response of various sizes of industrial grade MoS<sub>2</sub> which are produced in a similar fashion to large scale production was undertaken. To establish the mechanisms of cellular interactions and to assess any potential health impacts, three possible exposure routes (inhalation, ingestion and intravenous injection) were investigated in the physiologically relevant representative cell lines. A549, AGS and THP-1 were used as the three representative cell lines to mimic the possible exposure routes and for consistency with other studies with nanomaterials (36).

MoS<sub>2</sub> sheets fabricated for the purpose of this study are industrial grade and produced in a non-sterile fashion, similar to 2D material synthesis when used in applications for electronic devices. In this “bucket style” chemistry manufacturing of nanomaterials, contamination is inevitable and must be investigated to determine what effect it has on nanomaterial characteristics and what toxicity occurs following cellular exposure. Endotoxin, or more commonly known as lipopolysaccharide (LPS) is a large contributor to contamination of nanomaterials and when present can act as a stimulator of the inflammatory system (37,38). Nanoflakes produced for this study are different to the standard nanomaterials used for environmental nanosafety assessments (39). Nanomaterial samples of different sizes, originating from different batches and synthesised by varying individuals in this form demonstrates that material prepared in a commercial and large scale industrial setup will not produce endotoxin free MoS<sub>2</sub> samples. Therefore, the work illustrated within this paper demonstrates the toxicity observed after the realistic exposure to nanomaterials in the manufacturing environment of MoS<sub>2</sub>. Endotoxin screening is crucial to accurately understand whether cellular responses are from nanomaterials or nanomaterial-endotoxin coated materials.

## Materials and methods

### 2D MoS<sub>2</sub> Production

Full characterisation of MoS<sub>2</sub> nanosheets fabricated by the same method has previously been published by some of the co-authors (4,10,40). MoS<sub>2</sub> flake production is briefly outlined below.

Molybdenum disulphide powder (Sigma Aldrich, Ireland) was sonicated in aqueous surfactant solution (sodium cholate (SC), 6 g/l) for 1 h. The resultant dispersion was centrifuged at 5 krpm for 90 min to remove any impurities in the starting powder. The supernatant was discarded, while the sediment was re-dispersed in fresh aqueous SC solution (0.5 g/l) and sonicated for 6 h to produce a stock dispersion. The stock dispersion is quite polydisperse, and therefore to achieve a well-defined nanosheet size distribution, the sample was subjected to liquid cascade centrifugation (LCC).

LCC is a series of progressively increasing centrifugation speeds which produces narrowly distributed nanosheet sizes in solution. To produce varying nanosheet sizes in solution, the stock dispersion was initially centrifuged at 1 krpm for 90 min to remove any unexfoliated material. The sediment was discarded while the supernatant was collected and centrifuged at a higher speed (1.5 krpm for 90 min). After centrifugation at 1.5 krpm, the sediment was collected and redispersed in fresh aqueous SC (0.5 g/l), which represents the first nanosheet size selection. The supernatant was subjected to the next highest speed, 2.5 krpm for 90 min. Similarly the sediment was collected and redispersed in aqueous SC while the supernatant was centrifuged at a higher speed. This process was repeated for 2.5 krpm, 3.5 krpm, 5 krpm and 10 krpm. The respective sediments for a given speed were analysed using UV- vis spectroscopy and electron microscopy to determine the nanosheet concentration and mean lateral size (9). LCC maximises the nanosheet concentration of the nanosheets in solution in addition to producing a range of narrow nanosheet size distributions ranging from 50 nm to 177nm mean flake length.



## **TEM Material Characterization**

Bright-field transmission electron microscopy image was performed using a JEOL 2100 operated at 200 kV. Holey carbon grids (400 mesh) were purchased from Agar Scientific and prepared by diluting dispersion to a low concentration and drop-casting onto a grid placed on a filter membrane to wick away excess solvent. The grids were then baked at 120 °C to remove all solvent.

## **UV-Vis Spectroscopy**

(a) Material Characterization: Optical extinction was measured on a Varian Cary 5000 in quartz cuvettes with a path length of 0.4 cm for all three sizes. If necessary, the dispersions were diluted by pure solvent immediately prior to the measurement to yield optical densities below 1.5.

(b) Material stability in media: Three representative MoS<sub>2</sub> sizes were diluted in sodium cholate (0.5 mg/ml), phenol free RPMI media supplemented with 10% FBS, 1% penicillin-streptomycin and sodium chloride (40 mg/ml) in 96-well plates (Nunc, Fisher Scientific, Ireland). Sample absorbance was measured at time 0, 24, 48, 72 and 96 h using Spectramax M3 plate reader (Molecular Devices, USA).

## **Cell Culture**

Human acute monocytic leukaemia (THP-1) cells were obtained from the American Tissue Culture Collection (ATCC). THP-1 cells were cultured in Roswell Park Memorial Institute (RPMI) medium (Gibco, Bio-sciences Ltd, Ireland) supplemented with 10% Foetal Bovine Serum (FBS) (Sigma Aldrich, Ireland) and 1% penicillin-streptomycin (Sigma Aldrich, Ireland) in a humidified atmosphere at 37 °C and 5% CO<sub>2</sub>. THP-1 cells were differentiated into macrophage-like cells by incubating them with 200 nM phorbol 12-myristate 13-acetate

(PMA). THP-1 cells were removed from cell culture flasks, collected in a 15 ml tube (Fisher Scientific, Ireland) and centrifuged at 4,000 rpm for 5 min. Cells were counted using an automated Countess cell counter (Fisher Scientific, Ireland) and seeded at a density of  $1 \times 10^5$  cells/ml ( $5 \times 10^4$  cells/well; 500  $\mu$ l/well) in a 6-well (TEM), 24-well (along with glass coverslips for cell staining and laser scanning confocal microscopy) or 96-well (Live/Dead and high content screening) plate (Nunc, Fisher Scientific, Ireland) along with a stock solution of 60 ng/ml of PMA (30 ng/ well; 500  $\mu$ l/well) for 72 h at 37 °C and 5% CO<sub>2</sub>. Media and PMA were removed after 72 h and cells were washed with pre-warmed phosphate buffer saline (PBS) (Fisher Scientific, Ireland). MoS<sub>2</sub> nanomaterial solutions were diluted in supplemented culture media and added to macrophage-like THP-1 cells (500  $\mu$ l/well).

Human lung adenocarcinoma (A549) and human gastric adenocarcinoma (AGS) cells were obtained from ATCC. A549 and AGS cells were cultured in Ham's F-12 Kaighns Modified Medium (F-12K) supplemented with 10% FBS (Sigma Aldrich, Ireland) and 1% penicillin-streptomycin (Sigma Aldrich, Ireland) in a humidified atmosphere at 37 °C and 5% CO<sub>2</sub>. Cells were incubated for 24 h to allow cell attachment to Nunc culture flasks (Nunc, Fischer Scientific, Ireland) or until 60 – 80% confluency was achieved before splitting again. Medium was removed from cell culture flasks, cells were washed with pre-warmed PBS and detached using 2 ml TrypLE (Gibco, Bio-sciences Ltd, Ireland) in a T75 cm<sup>2</sup> culture flask for 5 – 8 min at 37 °C. TrypLE was neutralized with 6 ml supplemented culture media and collected in a 15 ml tube (Fisher Scientific, Ireland) and centrifuged at 4 krpm for 5 min. Cells were counted using an automated countess cell counter (Fisher Scientific, Ireland) and seeded at a density of  $1 \times 10^5$  cells/ml ( $5 \times 10^4$  cells/well; 500 $\mu$ l/well) in a 6-well (TEM), 24-well (along with glass coverslips for cell staining and laser scanning confocal microscopy) or 96-well (Live/Dead and high content screening) plate (Nunc, Fisher Scientific, Ireland) plate. Cells were grown for 24 h to allow cell attachment before exposure to nanomaterials diluted in the appropriate media.

### **High content screening (HCS)**

Cells were seeded in 96-well Nunc plates, incubated for 24 h at 37 °C, 5% CO<sub>2</sub> and exposed to linearly increasing concentrations of MoS<sub>2</sub> nanomaterials. Cells exposed to

medium, nocodazole and SC surfactant were also included as controls. Cells were then washed with pre-warmed PBS to remove dead and dying cells and fixed for 15 min at room temperature using a 4% PFA solution. Fixative solution was removed by two wash steps using 200  $\mu$ l/well of pre-warmed PBS. Cellular nuclei were stained for 10 min at ambient temperature using diluted (1-in-5000) nuclear stain Hoechst (Hoechst 33342, Thermo Fisher) and incubated in the dark. Staining solution was removed and cells were washed twice with 200  $\mu$ l/well of pre-warmed PBS. Cells were imaged by high content screening using the GE blue INcell 100 system. Nuclei were visualized using the blue channel of  $\lambda_{\text{exc}} = 405$  nm for the Hoechst nuclear dye. Ten fields per well were acquired using a 10x objective lens and simultaneously counted for each well. Dose-response graphs are fitted using the untreated (NT) as the 100% normalized cell population.

### **Live/Dead Viability Assay**

THP-1, A549 and AGS cells were seeded in 96-well Nunc treated plates and exposed for 24, 48 and 72 h at 37 °C, 5% CO<sub>2</sub> to increasing concentrations of MoS<sub>2</sub> nanomaterial (0.5, 2, 10  $\mu$ g/ml). Cells exposed to medium, nocodazole, methanol and SC surfactant were also included as controls. LIVE/DEAD® Viability/Cytotoxicity Kit for Mammalian Cells (Thermo Fisher, L3224) was used. Following exposure to the MoS<sub>2</sub> nanomaterials, the cells were rinsed with pre-warmed sterile PBS. The cells were then incubated with the Live/Dead solution containing Calcein AM and Ethidium homodimer-1 for 45 minutes as per the manufacturer's guidelines. The plates were then imaged using a confocal microscope (Zeiss LSM 510, 20x objective lens,  $\lambda_{\text{exc}} = 488$  nm for calcein AM and  $\lambda_{\text{exc}} = 561$  nm for Ethidium homodimer-1).

### **Cell staining and laser scanning confocal microscopy (LSCM)**

MoS<sub>2</sub> was diluted accordingly in the appropriate media for each cell and exposed to cells for 4 or 24 h incubation time points. Following exposure in 24-well plates, medium was removed and cells were washed with 500  $\mu$ l pre-warmed PBS. Cells were fixed using a 4% solution of paraformaldehyde (PFA (Sigma Aldrich, Ireland); 500  $\mu$ l/well) and incubated at

room temperature for 15 min. Triton X, at a concentration of 0.03%, was used for cell permeabilization for 3 min at room temperature with subsequent PBS washes. Cells were stained for 2 h at room temperature with Hoechst (Invitrogen, Oregon, USA), rhodamine phalloidin (Invitrogen, Oregon, USA) and anti- $\alpha$  tubulin Alexa 488 (Invitrogen, Oregon, USA) diluted accordingly to the manufactures instructions. Coverslips containing adherent and stained cells were removed and mounted on glass slides using fluorescence mounting medium (Dako Diagnostics Ireland Ltd.) and allowed to dry in the dark overnight. Cell nuclei (blue), F-actin filaments (red) and tubulin structures (green) were visualized using ZEISS 510 Meta confocal microscope (Carl Zeiss, Germany).

### **TEM Cellular Imaging**

Samples for transmission electron microscopy were first fixed in 2.5% glutaraldehyde in 0.1M Sørensen's phosphate buffer for a minimum of 2 h at room temperature and post fixed in 1% osmium tetroxide in Sørensen's phosphate buffer for 1 h at room temperature. Subsequently, the specimens were dehydrated in a graded ethanol series (30%, 50%, 70%, 90% and 100%). When dehydration was complete, samples were transferred from 100% ethanol to a mixture of 1 part of ethanol and 1 part of epoxy resin for 1 h. To complete the resin infiltration, the samples were placed in 100% resin at + 37 °C for 2 h. Finally, samples were embedded in resin, placed at + 60 °C for 24 h to complete polymerisation. For orientation purposes, 500 nm sections were cut from each sample, stained with toluidine blue, and examined by light microscopy (Leica DMLB, Leica Microsystems, Germany). From these survey sections, areas of interest were identified and ultrathin (80 nm) sections were cut using a Leica EM UC6 ultramicrotome (Leica Microsystems, Wetzlar, Germany). These sections were collected on 200 mesh thin bar copper grids, stained with uranyl acetate for 20 min, lead citrate for 5 min and examined by transmission electron microscopy (Tecnai G2 12 BioTWIN using an accelerating voltage of 120kV).

### **Endotoxin Detection by endpoint chromogenic LAL assay**

Pierce® LAL Chromogenic Endotoxin Quantitation kit (Thermo Scientific) was used to determine endotoxin levels found in MoS<sub>2</sub> samples (1 µg/ml). The endotoxin calibration curve was prepared using reconstituted stock solution of LPS from *Escherichia coli* (*E.coli*). Dilutions were performed as indicated in the protocol provided by the manufacturer. Briefly, dilutions of standards, nanoparticle stock solutions and solvents were prepared in endotoxin free water supplied by manufacturers. All samples were tested in duplicate. Nanoparticle stock solutions and solvents were incubated with and without the presence of LAL chromogenic substrate to determine any inference in the assay due to MoS<sub>2</sub> nanomaterials, which was subtracted from the average absorbance for each sample to accurately determine the LPS contamination. Absorbance was measured at 405 nm to quantify the presence of endotoxin.

#### **Cytokine Detection using multiplex assay**

Following 24 h exposure of differentiated THP-1, AGS and A549 cells to three sizes (50 nm, 117 nm and 177 nm) of MoS<sub>2</sub> at varying concentrations, the supernatants were removed and stored at -80°C until further analysis. Supernatants were defrosted and diluted with assay diluent as per the manufacturer's instructions. A panel of human pro-inflammatory cytokines were evaluated using V-Plex Pro-inflammatory Panel 1 (human) Kit (catalogue no. K15049D) and the protocol was carried out as per supplier's instructions.

#### **Measurement of Dendritic Cell Activation**

Age-matched, 6-8 weeks endotoxin hyporesponsive C3H/HeJ or wild-type C3H/HeN were bred in the Trinity Biomedical Sciences Institute (TBSI) Bioresources Unit, Trinity College Dublin (TCD). Animals were maintained according to the regulations of the European Union and the Irish Department of Health. All animal studies were approved by the TCD Animal Research Ethics Committee (Reference Number 091210).

Murine bone marrow-derived dendritic cells (BMDC) were generated as described previously (41). Briefly, bone marrow cells were isolated from tibias and femurs of mice. Cells were grown in RPMI 1640 medium (Biosera, Boussens, France) supplemented with 8 %

ultra-low endotoxin heat-inactivated FBS (Biosera), 2 mM L-glutamine (Gibco, Dun Laoghaire, Ireland), 50 U/mL penicillin (Gibco), 50 µg/mL streptomycin (Gibco) and 20 ng/mL of granulocyte–macrophage colony-stimulating factor (GM-CSF) derived from the J588 myeloma cell line. On day 10 the loosely adherent cells were harvested and plated at a density  $0.625 \times 10^6$  cells/mL and stimulated with MoS<sub>2</sub> particles as indicated in figure legends. Supernatants were collected and analysed for cytokine secretion and cells harvested for flow cytometry analysis.

### **Isolation and culture of murine bone marrow-derived dendritic cells**

As previously mentioned and described (41).

### **Cell Viability and cytokine levels of BMDC's**

For the analysis of cellular viability, cells were incubated with LIVE/DEAD® fixable Aqua Dead Cell Stain (Invitrogen, Dun Laoghaire, Ireland). Samples were acquired on BD FACSCanto II (BD Biosciences, USA) and the data analysed using FlowJo software (Tree Star Inc., Ashland, OR, USA). The concentration of the cytokine IL-6 was measured by ELISA using antibodies obtained from Biolegend (San Diego, CA, USA) according to the manufacturer's instructions.

## **Results**

### **High Content Screening**

HCS is an automated high throughput microscopy technique allowing for rapid imaging and subsequent analysis of large sample sets, permitting rapid toxicity assessments to be evaluated for nanomaterial exposure. Nuclear regions of cells were stained using Hoechst dye, allowing cell viability and toxic nanomaterial concentrations to be determined for each cell line. A range of concentrations (0, 0.5, 1, 2, 5 and 10 µg/ml) were tested for all three samples on all three cell lines (**Figure 1**). High content analysis (HCA) showed a minor changes in the number of viable A549 cells after interaction with five concentrations of nanomaterial of each size for 24 h. AGS cells were susceptible to toxicity after exposure to the highest concentration for 24 h, cell viability decreasing to <50%. THP-1 cells appear the most susceptible to toxicity of the MoS<sub>2</sub> material, exhibiting an increased cell death with

increasing concentration after 24 h exposure. Levels of cell number in THP-1 cells show large variability, beyond the standard deviation level. Nuclear morphology in differentiated THP-1 cells can vary from single (circular) to multi-lobed (irregular shaped), as can be seen from images in other studies (8–10), which can lead to an inaccurate cell count based on a nuclear stain. Therefore, when cell number was obtained following analysis of the THP-1 data, software misinterpretation is most likely the cause of fluctuation in these cell numbers. AGS cells were most susceptible to 117 nm MoS<sub>2</sub> at 10 µg/ml, while THP-1 show the highest toxicity towards the smallest MoS<sub>2</sub> sheets (50 nm).

**Comment [HB1]:** You need to comment on the variability of this here

**Comment [HB2]:** Have these been included?

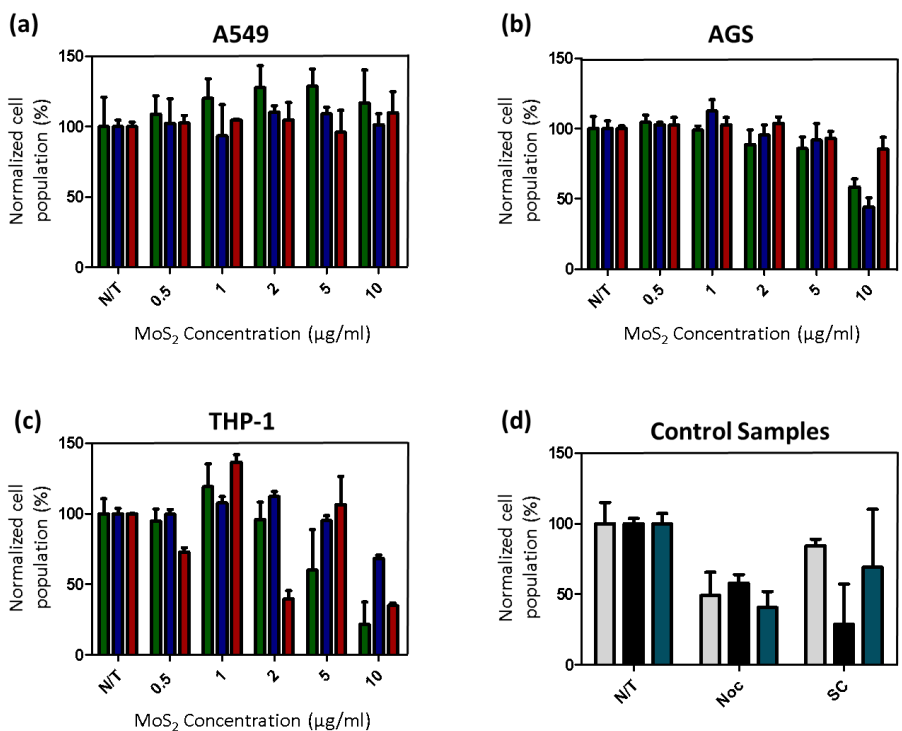


**Figure 1** Cell viability as determined by high content screening. Particle concentrations (0.5, 1, 2, 5 and 10 µg/ml) were added to a) A549 cells, b) AGS cells and c) THP-1 cells for 24 h. Figure a-c: green – 50 nm, blue – 117 nm and red 177 nm. Figure d: grey – A549, black – AGS and blue – THP-1. Control samples as illustrated in figure d: NT – negative treatment, Noc – Nocodazole and SC- Sodium Cholate.

### Live/Dead Cell Viability Assay

The Live/Dead assay enables the assessment of nanomaterial toxicity by examining cells by confocal microscopy after incubation with varying concentrations of nanomaterials

and subsequent incubation with fluorescent markers discriminating between live and dead cells. Untreated (viable) cells absorb the calcein AM dye to fluoresce green when excited and examined under a microscope. Cells treated with 70% methanol prior to staining show no viable cells, all cells fluorescing red after interaction with the ethidium homodimer-1 dye. Although the A549 and AGS cell images are acquired at a higher cell density, it is notable that the MoS<sub>2</sub> nanomaterials at the elevated concentration (10 µg/ml) elicit minor amounts of cytotoxicity (**Figure 2**). In contrast, THP-1 cells show increased cytotoxicity when exposed to MoS<sub>2</sub> nanomaterials at a concentration of 10 µg/ml, resulting in increased cell death compared to the untreated control. The equivalent amount of SC surfactant present in 10 µg/ml of MoS<sub>2</sub> was also tested and toxicity was observed when SC is free in solution. Although, it should be noted that the effective concentration and molecular organisation of SC free in solution and organised on a nanosheet surface is very different, and a direct comparison is not possible. While only the effects of the highest concentration (10 µg/ml) are presented for each nanomaterial size in **Figure 2**, a range of concentrations was tested with all cell lines (**Supplemental 4(a) – (d)**) over three time-points (24, 48 and 72 h), confirming 1 µg/ml is a sub-lethal and non-toxic concentration over a 24 h time period.

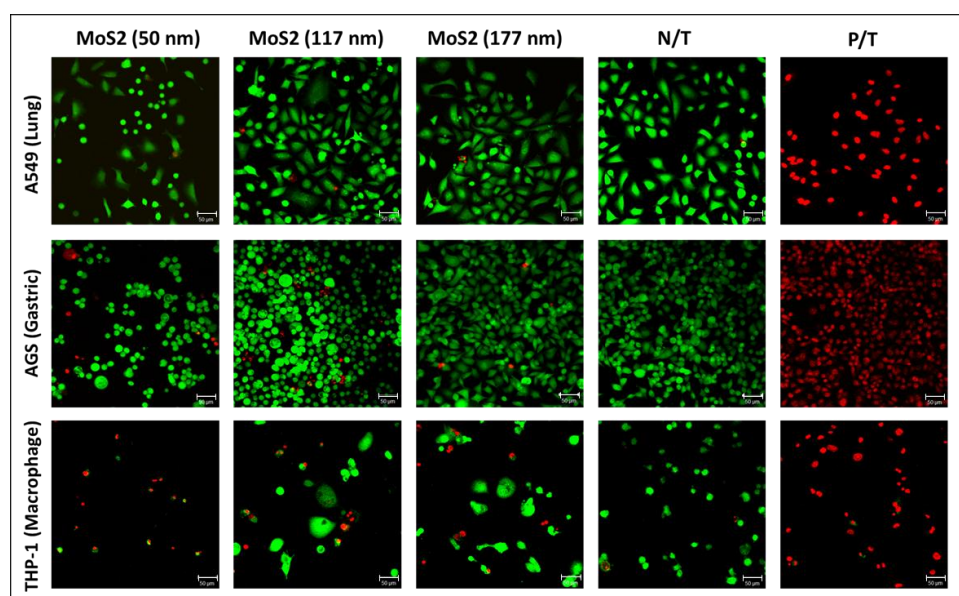


**Figure 2** Live/Dead cell viability images of untreated A549, AGS and THP-1 cells and following 24 h exposure to 10 µg/ml of three sizes of MoS<sub>2</sub> nanomaterial (50 nm, 117 nm and 177 nm). Images were acquired on a Zeiss LSM 5 10 confocal



microscope under low magnification (x20 objective lens). Green – live cells and red – dead/dying cells. Control samples as indicated by N/T – negative treatment and P/T – positive treatment. (Scale bar 50  $\mu\text{m}$ ).

### **Laser Scanning Confocal Microscopy (LSCM)**

In order to explore the cell morphology in greater detail confocal microscopy was carried out. It allows for the visualisation and characterisation of cells with increased optical resolution compared to conventional light microscopy. Using cytoskeletal stains for F-actin (rhodamine phalloidin: red), tubulin (anti- $\alpha$  tubulin alexa 488: green) and a nuclear stain (Hoechst: blue), intracellular structures were imaged and analysed to identify any cellular and/or morphological changes between treated and untreated cells. Cell adhesion characteristics, cytoskeletal and nuclear morphologies were explored using LSCM of cells exposed to a concentration of 1  $\mu\text{g}/\text{ml}$ . Cells were inspected for characteristics such as loss in membrane integrity, cell lysis, shrinkage of cytoplasmic regions or cell fragmentation, as an indication of necrosis and/or apoptosis.

In the case of A549 and AGS cells, there were no signs of necrosis, apoptosis or acute toxicity, as evidenced by the absence of cytoplasmic swelling or membrane blebbing, following a 24 h exposure (**Figure 3**). Resting THP-1 cells were spherical in shape, with round intact nuclear regions and actin arrangements on the periphery of the cells. Following exposure to  $\text{MoS}_2$ , pseudopodial extensions with actin and tubulin rearrangement can be observed in differentiated THP-1 cells after a 4 h incubation (**Supplemental Figure 4**) and an increased number of interacting THP-1 cells after a 24 h incubation. Cells were also exposed to the equivalent amount of SC surfactant in 1  $\mu\text{g}/\text{ml}$  of  $\text{MoS}_2$ , to confirm that no toxicity, necrosis and/or apoptosis has been caused by this surfactant.

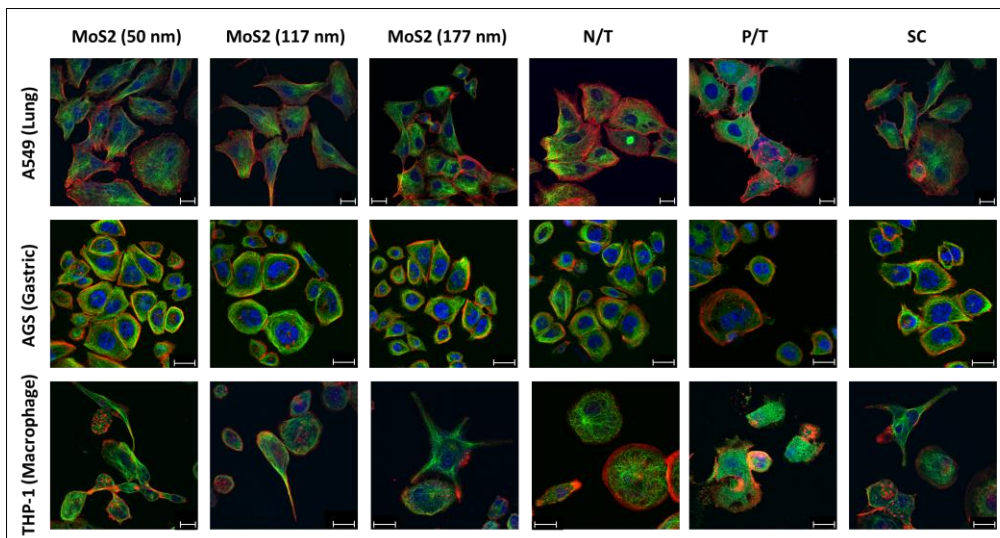


**Figure 3** Confocal microscopic images of untreated THP-1, AGS and A549 cells and following 24 h exposure to 1 µg/ml of three different MoS<sub>2</sub> nanomaterial sizes (50 nm, 117 nm and 177 nm). Images were acquired on a Zeiss LSM 5 10 confocal microscope under oil immersion (63x magnification). Red – F-actin, green – α-tubulin and blue –nucleus. N/T – negative treatment control, P/T – positive treatment, SC – sodium cholate (scale bars: 20µm).

### Transmission Electron Microscopy (TEM)

Transmission electron microscopy was used to explore nanomaterial uptake within the cells. To observe possible MoS<sub>2</sub> uptake with minimal toxic effects the cells were treated with 1 µg/ml of MoS<sub>2</sub> over a 24 h time period (which was established as a sub-lethal concentration using HCS and Live/Dead analysis). A549, AGS and differentiated THP-1 cells were exposed to a concentration of 1 µg/ml of MoS<sub>2</sub>, diluted in the appropriate medium and exposed for 4 and 24 h. Representative cellular images in **Figure 4**, following 24 h incubation with MoS<sub>2</sub> nanomaterials, confirms uptake of all three sizes of MoS<sub>2</sub> in all three cell lines. The internalisation of MoS<sub>2</sub> material of each of the three sizes can be seen, as indicated by the red arrows in the figure. Internalisation of material was also observed at an earlier exposure time-point of 4 h (data not shown). In all cases, the nanomaterials appear to be located in single membrane vesicles within the cell, consistent with endosomal or lysosomal cell trafficking (42). There are no signs of any sub-cellular damage or toxicity.

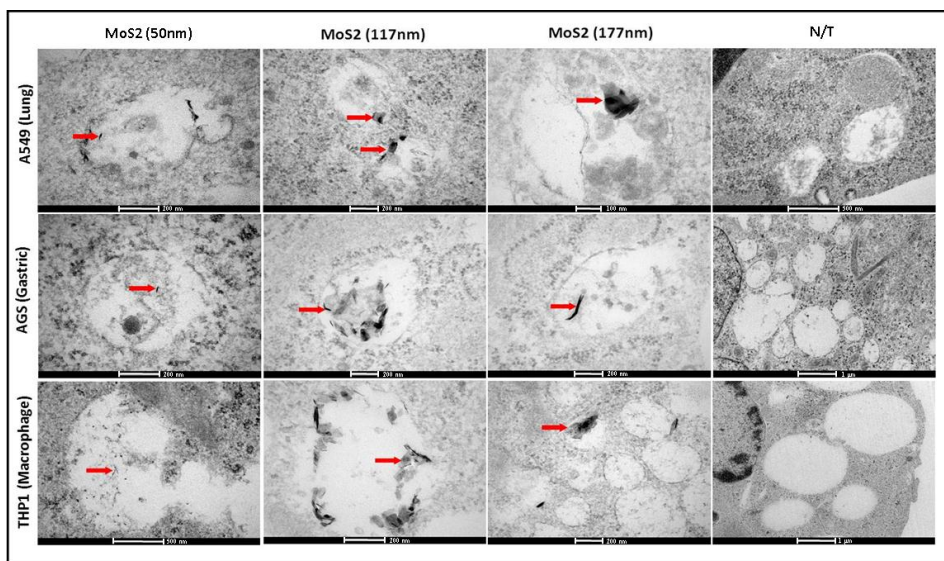


**Figure 4** Electron microscopy images of three different cell lines (THP-1 macrophage-like cells, AGS gastric cells and A549 lung cells) following 24 h exposure to 1  $\mu\text{g}/\text{ml}$  of three different sizes of  $\text{MoS}_2$  (50 nm, 117 nm and 177nm). Nanomaterial uptake is observed in all three cells lines and is indicated by the red arrows, where the nanomaterials are located in single membrane vesicles.

### Endotoxin Detection

The presence of endotoxin contaminates adsorbed onto nanomaterial surfaces can modify the immune and cellular responses following cellular interaction with foreign bodies (43). To accurately understand the toxic response of cells to  $\text{MoS}_2$  nanomaterials, the presence of endotoxin must be established. Endotoxin contamination was detected in all three  $\text{MoS}_2$  nanomaterials used, levels in all cases exceeding the lower limit of detection of the kit used (0 - 1 EU/ml).  $\text{MoS}_2$  suspensions at the same concentration were incubated with and without the presence of substrate as supplied by manufacturers to determine any optical interference caused by nanomaterial's with the assay. Interference is detected following the production of a chromogenic yellow colour in the absence of substrate. Notably, no interference was detected when  $\text{MoS}_2$  suspensions were incubated with the assay. Sodium cholate (SC) surfactant also tested positively for the presence of endotoxin (**Figure 5a**). The assay confirms that endotoxin contamination originates from both nanomaterials and surfactants. Looking at **Figure 5b**, it can be seen that, as nanomaterial

surface area increases, the endotoxin content per surface area, for a fixed exposure concentration of 1  $\mu\text{g}/\text{mL}$ , decreases (44,45). Therefore, a relationship between the quantity of endotoxin detected and the available nanomaterial surface edge is indicated, suggesting that the edge states are the primary binding sites for endotoxins.

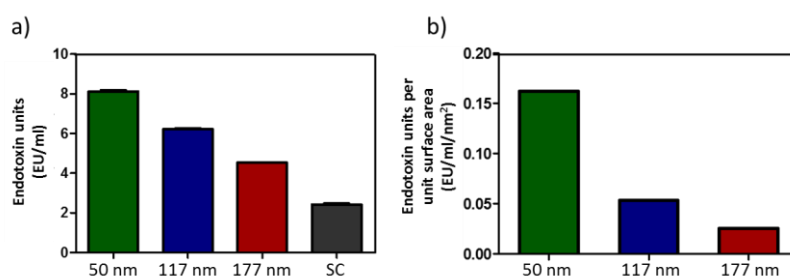


**Figure 5** Endotoxin detection of nanomaterial samples. a) Illustrates the extrapolated value of endotoxin present in all samples. Figure 5b demonstrates the relationship between increasing nanomaterial surface edge and increasing endotoxin presence on the surface.

### Multiplex assessment of cytokine secretion

Assessment of cytokine secretion by cells following exposure to a non-toxic nanomaterial concentration provides an indication of immune cell activation. A panel of ten cytokines were analysed on diluted supernatants of cells exposed to  $\text{MoS}_2$  nanomaterial using an MSD 10-spot ELISA assay. Standards could be measured and calculated accurately, although some supernatant samples were above or below the limits of detection. Macrophage-like THP-1 cells showed an enhanced cytokine production after exposure to nanomaterials when compared to the A549 and AGS cell lines. Activated THP-1 cells showed a concentration and size dependent response for IL-6, IL-10, IL-13, TNF- $\alpha$  and IL-1 $\beta$  secretion after exposure to  $\text{MoS}_2$  (**Figure 6**). A correlation between cytokine levels produced and available nanomaterial surface area (including increased endotoxins present) could be observed clearly with THP-1 cells.

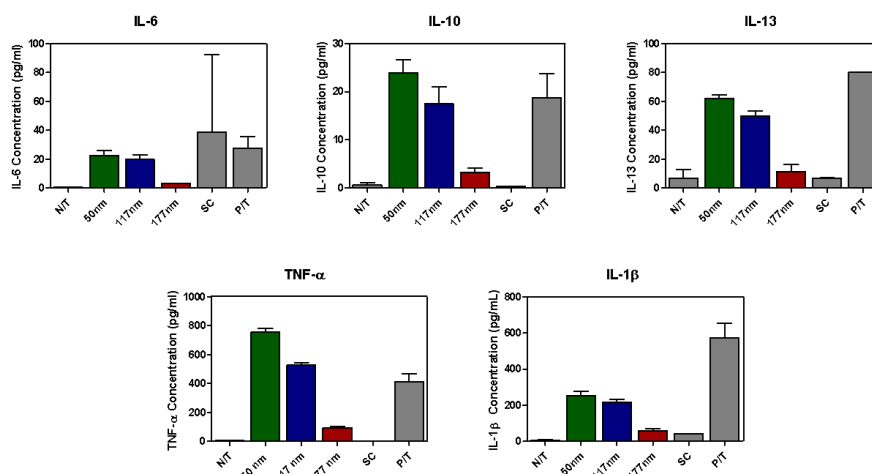


**Figure 6** IL-6, IL-10, IL-13, TNF- $\alpha$  and IL-1 $\beta$  cytokine responses of THP-1 cells as determined by MSD multi-plex 10-spot pro-inflammatory ELISA kit. Cytokine response shown is recorded from supernatants of THP-1 cells following 24 h exposure to 1  $\mu\text{g}/\text{ml}$  of MoS<sub>2</sub> nanomaterial (50 nm, 117 nm and 177 nm). Green – 50 nm, blue – 117 nm, red – 177 nm, grey – controls (N/T – Not treated, SC – Sodium Chololate, P/T – positive treated).

### BMDC viability as determined by flow cytometry

Depending on the integrity of the plasma membrane, the Aqua Dead cell stain functions by interacting with free amines on the cell surface or in the interior of the cell. BMDC's viability was evaluated to confirm 1  $\mu\text{g}/\text{ml}$  is a sub-lethal and non-toxic concentration prior to investigating IL-6 cytokine responses from wild-type and TLR4 defective BMDC's are primary cells which may be more susceptible to damage from foreign material than the immortalized cell lines already tested. Cell viability was analysed following exposure to 1  $\mu\text{g}/\text{ml}$  of MoS<sub>2</sub> for 24 h. No cell death was evident following exposure to three sizes of MoS<sub>2</sub> (**Figure 7**). Exposure to SC solution (60  $\mu\text{g}/\text{ml}$ ) resulted in a minor decrease in cell viability, indicating cell membranes were damaged in a small proportion of the population.

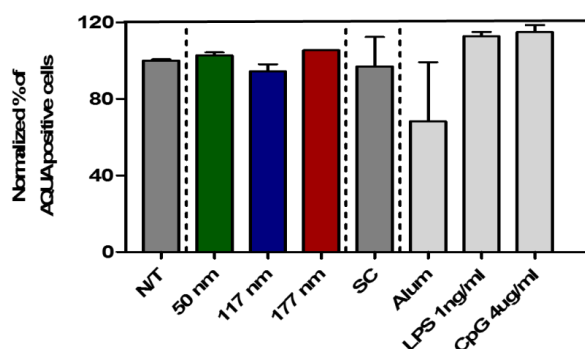


**Figure 7** Cell viability of BMDC's as determined by LIVE/DEAD fixable aqua dead cell stain and analysed using flow cytometry. Viability illustrated is BMDC's following 24 h exposure to 1  $\mu\text{g/ml}$  of  $\text{MoS}_2$  nanomaterial (50 nm, 117 nm and 177 nm). Controls as illustrated are N/T – negative treatment, SC – sodium cholate, Alum – 500 mg/ml, LPS – Lipopolysaccharide and CpG – 4  $\mu\text{g/ml}$ .

### BMDCs cytokine response

In wild type (C3H/HeN) dendritic cells, LPS triggers activation via TLR4 signalling leading to secretion of cytokines including IL-6. Cell derived from C3H/HeJ mice are hypo-responsive to LPS and here are used to provide an indication of LPS contamination in  $\text{MoS}_2$  nanomaterials. The IL-6 cytokine results obtained from BMDC's further confirm the findings from the LAL chromogenic assay, verifying cellular responses are a result of interaction with LPS contamination, nanomaterial suspensions and stabilising surfactant. Looking at **Figure 8**, all  $\text{MoS}_2$  sizes showed trivial IL-6 production following exposure to 1  $\mu\text{g/ml}$  of  $\text{MoS}_2$  in HeN cells, demonstrating a minor inflammatory reaction occurs in BMDC's following exposure to a sub-lethal concentration of  $\text{MoS}_2$ . Thus, at a concentration of 1  $\mu\text{g/ml}$ , TLR4 active HeN cells recognise  $\text{MoS}_2$  nanosheets as a foreign substance and initiate IL-6 cytokine production as an immune response. Up until this, it could not be confirmed whether toxicity, cellular responses or inflammation were due to nanomaterials, stabilizing surfactant or endotoxin bound to the nanomaterial surface. Therefore, to determine if cell responses are solely because of contaminating endotoxin, HeJ LPS hypo-responsive BMDC's were exposed to the same concentration of  $\text{MoS}_2$  for 24 h. **Figure 8** illustrates that LPS loaded  $\text{MoS}_2$  nanomaterials promote higher levels of cytokine secretion while little or no cytokine is produced by LPS hypo-responsive C3H/HeJ cells. Consequently, this reveals

toxicity and cellular responses are not solely associated to MoS<sub>2</sub> nanoflakes but also with contaminating LPS on the surface attached during nanomaterial production.

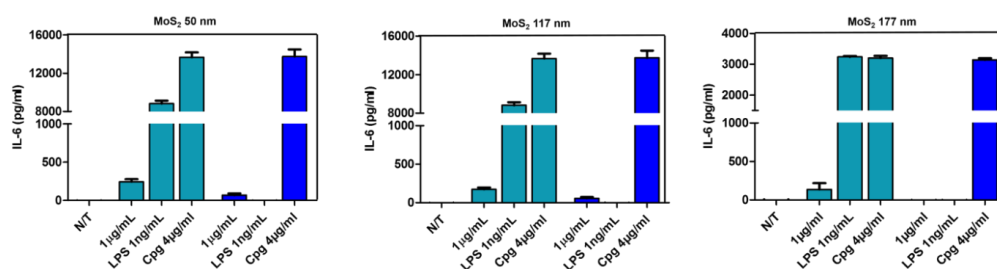


**Figure 8** IL-6 concentrations in supernatants from (C3H/HeN) and LPS hyporesponsive C3H/HeJ BMDC's collected following a 24 h exposure to 1 µg/ml of MoS<sub>2</sub> nanomaterial (50 nm, 117 nm and 177 nm).

## Discussion

Of the sparse cytotoxicity data published for MoS<sub>2</sub> nanosheets, toxicity has been measured using techniques such as 3-(4, 5-Dimethylthiazol-2-Yl)-2, 5-Diphenyltetrazolium Bromide (MTT) as a method to determine the metabolic activity of viable cells. However, it should be noted that MTT data on the cytotoxic effects triggered by exposure to nanomaterials lack reproducibility, due to the interference of nanomaterials with colorimetric assays (46). Therefore, we opted for a more extensive and elaborate toxicity screening assessment to accurately confirm and identify sub-lethal concentrations for the cell lines being tested. HCS and Live/Dead are high throughput techniques that allow images to be acquired and analysed to give a fast output of viable cell number.

A549 cells are human alveolar basal epithelial cells which function as permeable membranes to allow passive diffusion of metabolites through cellular tight junctions. High unsaturated fatty acid content is observed in the surfactant of alveolar basal epithelial cells which may aid in a protective barrier allowing A549 cells to be the most resistant to cellular damage as observed with HCS and Live/Dead (47). AGS are gastric cells that function as a protective barrier and aid in the digestion of ingested proteins and fats. These cells are robust against the interaction with many molecules and microbes, explaining why a

decrease in cell number was only observed in AGS cells after incubation with the highest MoS<sub>2</sub> concentration (10 µg/ml). Monocytes are white blood cells that migrate and differentiate into macrophages in tissue due to stimulation of the immune system. Macrophages function by recognising antigens on foreign substances and cellular debris to engulfing material and subsequently produce anti-inflammatory cytokines (48). Due to the function of differentiated THP-1 cells, increased toxicity encountered may be due to phagocytosis of nanosheets with the smallest MoS<sub>2</sub> material causing the highest amount of cell damage. Nuclear morphology in differentiated THP-1 cells can vary in shape and size, which may contribute to the variability in cell responses following analysis of cells stained with a nuclear stain for HCS. Live/Dead experimentation act as a further confirmation test showing 1 µg/ml is sub-lethal and non-toxic to all cells lines following 24 h exposure. A nanomaterial size-dependent reaction is observed with AGS and THP-1 cells showing the higher bio-incompatibility with MoS<sub>2</sub> sheets of 117 nm in size in AGS cells, while the 50 nm MoS<sub>2</sub> shows the highest toxicity in THP-1 cells. Therefore, no well-defined correlation of cellular response with physicochemical properties of the nanomaterials was apparent after incubation of three nanomaterial sizes in three cells lines, which leads to the question of whether foreign or non-nanomaterial substances are causing the varying cellular response.

Following incubation with 1 µg/ml, the cellular morphology and interaction with MoS<sub>2</sub> was visualised using LSCM and florescent probes. Cellular morphology will change under environmental stress, which may cause loss in membrane integrity or membrane blebbing. Therefore, LSCM provides a first indication of whether necrosis and/or apoptosis is induced following exposure to sub-lethal concentrations of MoS<sub>2</sub> (49,50). Nuclear morphology appears normal in all cell lines tested following 4 and 24 h incubation with 1 µg/ml of MoS<sub>2</sub>. F-actin and α-tubulin filaments are found in the cytoplasmic region of cells. Actin plays a crucial role in maintaining cell shape/adhesion and damage in their structure can prevent cell function immensely. During mitosis and cell division, there is an active rearrangement of tubulin structures to aid in appropriate transport and distribution of DNA. Staining for F-actin and α-tubulin allows the visualisation of cytoskeletal rearrangements due to exposure to nanomaterials. A549 and AGS cells treated with nanomaterials show no change in cellular morphology, on comparison to untreated cells. Resting macrophages are circular in shape, as shown in **Figure 3**, with actin (red) visualized at the peripheral of the



cell. Core to macrophage function, pseudopodial extensions are noticeably present after exposure to all sizes of MoS<sub>2</sub> with actin and tubulin (green) rearrangement prominent. Images acquired through LSCM further illustrate the clarification as to why we have a cell type-dependent toxicity.

TEM was used for the visualisation of cells after 24 h incubation with nanomaterial to investigate the uptake and possible cellular responses after interaction with MoS<sub>2</sub> nanosheets. Here we show, for the first time, internalisation of MoS<sub>2</sub> of three sizes was observed in all three cell lines, as models for three different exposure routes. Due to the cellular function of macrophages, it was expected that THP-1 cells would show the highest rate of internalisation, although no differences could be observed between the cell lines tested. Notably, however, true in vivo exposure scenarios should consider the role of local macrophages which would potentially prevent the exposure of non-phagocytic cells. Previously published data would suggest nanomaterial of 50 nm would have the greatest affect although no differences could be observed in this study between different cell lines or nanomaterial sizes (51).

Endotoxin contamination of nanomaterials can occur at synthesis, handling or fabrication processing steps with increased adsorption of pollutants and organic material with increasing surface area present on nanomaterial surface. Therefore, it is of great importance when assessing the toxicity of nanoparticles to distinguish between toxicity from MoS<sub>2</sub> nanoparticles or endotoxin present on the surface (37). The main contaminant contributing to high levels of endotoxin comes from the cell wall of gram negative bacteria such as *Escherichia coli* (*E.coli*) and is commonly known as LPS. LPS contains a lipid A component which is responsible for increased inflammatory cytokine secretion by macrophages and dendritic cells after the binding of LPS to the toll-like receptor 4 (TLR4) and MD2 complexes on cell surfaces (38). Mainly, the lipid A moiety component is a stimulator of the inflammatory immune system causing chronic inflammation or sepsis in autoimmune suppressed individuals and therefore controlling and/or eradicating contamination is vital to preventing infections in this scenario (52).

Endotoxin presence was detected in large quantities in all three sizes of MoS<sub>2</sub> material used throughout this study. These results further illustrate the realistic levels of

endotoxin present on 2D MoS<sub>2</sub> sheets manufactured in large scale production. The relationship between size and the potential surface area for binding with foreign substances is evident in **Figure 5a** showing increasing endotoxin presence with decreasing nanomaterial size. MoS<sub>2</sub> sheets with an LPS corona bound to the nanomaterial surface, denotes a cellular response is most likely from the LPS coating or the stabilising surfactant. LPS can bind to MoS<sub>2</sub> sheets in a multi-directional format aiding in a multitude of nanoparticle sizes differing from each other consequentially altering the cellular response (37,43). Estimated sizes of each nanomaterial are from the same stock samples analysed for endotoxin detection.

One method of removing the endotoxin from nanomaterial suspensions is to heat suspensions to very high temperatures for extended periods of time, although this method cannot be used for 2D nanomaterials, as it will alter nanosheet structures, causing destabilisation and produce material characteristics different to the original (53). Antibiotics such as polymyxin b sulfate cannot be used for endotoxin removal, as altering the salt concentration for samples stored in sodium cholate causes destabilisation and flocculation of MoS<sub>2</sub> sheets. Therefore, when it is crucial to have endotoxin free samples, as those used for *in-vivo* applications such as contrast imaging agents or drug delivery, endotoxin free reagents must be used from the outset, extra care being taken during synthesis. New emerging therapies of using polymer coated MoS<sub>2</sub> sheets as administered gene therapies for silencing up-regulated genes have shown little toxicity at high concentrations, although the importance for endotoxin free samples is evident for these forms of applications (15). For the purpose of MoS<sub>2</sub> used in electronic devices, the need for endotoxin free samples may not be so critical, as samples will not be used *in-vivo* and the method for large scale production cannot eliminate the endotoxin during mass production.

The cellular transport and final destination of MoS<sub>2</sub> nanosheets and/or by-products will differ in pathway activation and cytokine production. Due to the limitations of using a multi-test ELISA plate, a selection of cytokines were above or below the limits of detection, explaining why different cytokines are displayed for each cell line. A panel of cytokines produced by A549 and AGS cells as illustrated in **Supplemental Figure 5(a-c)** demonstrate trivial production when compared to untreated control samples. This further confirms the robustness and stealth of each cell line when compared to THP-1 cells as demonstrated in Live/Dead and HCS results. TNF- $\alpha$  is produced by a multitude of cells, but predominantly

macrophages, building the first line of defence against foreign substances while upregulating cytokines and prostaglandins (54). Interestingly, **Figure 6** demonstrates a size-dependent reaction in macrophages following exposure to 1 µg/ml of MoS<sub>2</sub>, the smallest size stimulating the highest cytokine response. This size-dependent reaction may be attributed to the increased endotoxin on the surface of nanomaterials as nanomaterial size decreases as seen in **Figure 5b**, and, as a consequence, altering the nanomaterial size can affect the cellular reaction (55).

Even though the samples tested throughout this study mimic the realistic exposure in the manufacturing environment, the clarification that cytokine responses are from LPS or the nanomaterial itself need to be investigated. Therefore, wild-type and TLR4 hyporesponsive BMDC's cells can aid in distinguishing if the cytokine response is from the LPS contamination. Cell viability was tested to confirm 1 µg/ml is a sub-lethal and non-toxic concentration to primary BMDC's. Little or/no cell death was observed as seen in **Figure 7**. SC stabilising surfactant did cause a minor decrease in cell number although the sample contains SC free in solution. SC binds to the surface of MoS<sub>2</sub> aiding in nanosheet stabilisation and reducing the available amount of active binding sites. Polymyxin B sulfate has been used in previous studies for the effective removal of endotoxin within nanomaterial samples although this method cannot be applied to our material due to nanosheets destabilisation. Wild-type BMDC's show a low level of IL-6 production when exposed to three sizes of MoS<sub>2</sub> nanomaterial following a 24 h incubation. When the TLR4 defective HeJ cells are exposed to the same samples, there is a decrease and/or abrogation in IL-6 secretion from all sizes tested (**Figure 8**). This reveals the LPS content is a major contributor to a proportion of the cytotoxicity and cytokine inflammatory responses following incubation with MoS<sub>2</sub> nanomaterial. Therefore, this illustrates the importance of understanding the precise bio-interaction of cells with nanomaterials, surfactants or contaminants.

## Conclusion

The uptake, cytotoxicity and inflammatory response of three representative cell line mimicking possible exposure routes (inhalation, A549; ingestion, AGS; monocyte, THP-1) to MoS<sub>2</sub> flakes of three sizes was explored here. Sub-lethal concentrations were determined

using HCS and a live/dead assay which indicated a non-toxic concentration of  $\leq 1 \mu\text{g/ml}$ . TEM confirmed the uptake of all  $\text{MoS}_2$  nanomaterials in all three cell lines after 24 h up to a dose of  $1 \mu\text{g/ml}$ . The nanomaterials were ultimately located in single membrane bound vesicles. Confocal microscopy showed no signs of necrosis and/or apoptosis at this exposure. Endotoxin presence was evaluated to understand the cellular response more precisely, results showed as nanomaterial size decreases, the available surface edge increases and ultimately so does the quantity of LPS present. A relationship between the quantity of endotoxin detected and the available nanomaterial surface edge was revealed. Inflammatory cytokines measured using a 10-spot ELISA proved that cells interact with  $\text{MoS}_2$  in a nanoparticle size and cell dependent manner. IL-6 cytokine production in HeJ and HeN BMDC's confirmed that the detected cellular responses can be induced by LPS contamination,  $\text{MoS}_2$  sheets, stabilizing surfactant and possibly other yet unknown contaminants. Therefore, this comprehensive study provides a better understanding to the bio-interaction of  $\text{MoS}_2$  material which is produced in the manufacturing environment in non-sterile conditions, with results confirming  $\text{MoS}_2$  nanoflakes of three sizes at a concentration of  $1 \mu\text{g/ml}$  are non-toxic in three cell lines even in the presence of LPS contamination.

### **Acknowledgements**

Supported by Advanced Materials and BioEngineering Research (AMBER), DIT Fiosraigh scholarship scheme and Science Foundation Ireland (SFI grant 11/PI/1108) for financial contribution to this manuscript. The authors declare that they have no competing interests.

### **References**

1. Pokropivny V V., Skorokhod V V. Classification of nanostructures by dimensionality and concept of surface forms engineering in nanomaterial science. Mater Sci Eng C.

2007;27(5–8 SPEC. ISS.):990–3.

2. Du Y, Yin Z, Zhu J, Huang X, Wu X-J, Zeng Z, et al. A general method for the large-scale synthesis of uniform ultrathin metal sulphide nanocrystals. *Nat Commun.* 2012 Nov 6;3:1177.
3. Hernandez Y, Nicolosi V, Lotya M, Blighe FM, Sun Z, De S, et al. High-yield production of graphene by liquid-phase exfoliation of graphite. *Nat Nanotechnol.* 2008 Sep 10;3(9):563–8.
4. Coleman JN, Lotya M, O'Neill A, Bergin SD, King PJ, Khan U, et al. Two-dimensional nanosheets produced by liquid exfoliation of layered materials. *Science.* 2011 Feb 4;331(6017):568–71.
5. Novoselov KS, Fal'ko VI, Colombo L, Gellert PR, Schwab MG, Kim K. A roadmap for graphene. *Nature.* 2012 Oct 10;490(7419):192–200.
6. Novoselov KS, Geim AK, Morozov S V, Jiang D, Zhang Y, Dubonos S V, et al. Electric field effect in atomically thin carbon films. *Science.* 2004 Oct 22;306(5696):666–9.
7. Tiwari JN, Tiwari RN, Kim KS. Zero-dimensional, one-dimensional, two-dimensional and three-dimensional nanostructured materials for advanced electrochemical energy devices. *Prog Mater Sci.* 2012 May;57(4):724–803.
8. Mak KF, Lee C, Hone J, Shan J, Heinz TF. Atomically thin MoS<sub>2</sub>: A new direct-gap semiconductor. *Phys Rev Lett.* 2010;105(13):2–5.
9. Varrla E, Backes C, Paton KR, Harvey A, Gholamvand Z, McCauley J, et al. Large-Scale Production of Size-Controlled MoS<sub>2</sub> Nanosheets by Shear Exfoliation. *Chem Mater.* 2015 Feb 10;27(3):1129–39.
10. Smith RJ, King PJ, Lotya M, Wirtz C, Khan U, De S, et al. Large-scale exfoliation of inorganic layered compounds in aqueous surfactant solutions. *Adv Mater.* 2011;23:3944–+.
11. Ganatra R, Zhang Q. Few-layer MoS<sub>2</sub>: a promising layered semiconductor. *ACS Nano.* 2014 May 27;8(5):4074–99.

12. Radisavljevic B, Radenovic A, Brivio J, Giacometti V, Kis A. Single-layer MoS<sub>2</sub> transistors. *Nat Nanotechnol.* 2011 Mar 30;6(3):147–50.
13. Jariwala D, Sangwan VK, Lauhon LJ, Marks TJ, Hersam MC. Emerging Device Applications for Semiconducting Two-Dimensional Transition Metal Dichalcogenides. *ACS Nano.* 2014 Feb 25;8(2):1102–20.
14. Spadavecchia J, Movia D, Moore C, Manus Maguire C, Moustaooui H, Casale S, et al. Targeted polyethylene glycol gold nanoparticles for the treatment of pancreatic cancer: from synthesis to proof-of-concept in vitro studies. *Int J Nanomedicine.* 2016 Feb;Volume 11:791.
15. Kou Z, Wang X, Yuan R, Chen H, Zhi Q, Gao L, et al. A promising gene delivery system developed from PEGylated MoS<sub>2</sub> nanosheets for gene therapy. *Nanoscale Res Lett.* 2014;9(1):587.
16. Wang S, Chen Y, Li X, Gao W, Zhang L, Liu J, et al. Injectable 2D MoS<sub>2</sub> -Integrated Drug Delivering Implant for Highly Efficient NIR-Triggered Synergistic Tumor Hyperthermia. *Adv Mater.* 2015 Nov;27(44):7117–22.
17. Saptarshi SR, Duschl A, Lopata AL. Interaction of nanoparticles with proteins: relation to bio-reactivity of the nanoparticle. *J Nanobiotechnology.* 2013;11:26.
18. Aggarwal P, Hall JB, McLeland CB, Dobrovolskaia MA, McNeil SE. Nanoparticle interaction with plasma proteins as it relates to particle biodistribution, biocompatibility and therapeutic efficacy. *Adv Drug Deliv Rev.* 2009;61(6):428–37.
19. Petros RA, DeSimone JM. Strategies in the design of nanoparticles for therapeutic applications. *Nat Rev Drug Discov.* 2010 Aug 9;9(8):615–27.
20. Braakhuis HM, Gosens I, Krystek P, Boere JA, Cassee FR, Fokkens PH, et al. Particle size dependent deposition and pulmonary inflammation after short-term inhalation of silver nanoparticles. *Part Fibre Toxicol.* 2014 Dec 17;11(1):49.
21. Oberdörster G, Sharp Z, Atudorei V, Elder A, Gelein R, Kreyling W, et al. Translocation of inhaled ultrafine particles to the brain. *Inhal Toxicol.* 2004 Jun;16(6–7):437–45.

22. Cheung DO, Halsey K, Speert DP. Role of pulmonary alveolar macrophages in defense of the lung against *Pseudomonas aeruginosa*. *Infect Immun*. 2000 Aug;68(8):4585–92.
23. Bergin IL, Witzmann FA. Nanoparticle toxicity by the gastrointestinal route: evidence and knowledge gaps. *Int J Biomed Nanosci Nanotechnol*. 2013;3(1–2).
24. Fröhlich E, Roblegg E. Models for oral uptake of nanoparticles in consumer products. *Toxicology*. 2012 Jan 27;291(1–3):10–7.
25. Lockman PR, Koziara JM, Mumper RJ, Allen DD. Nanoparticle surface charges alter blood-brain barrier integrity and permeability. *J Drug Target*. 2004;12(9–10):635–41.
26. Chen G-Y, Yang H-J, Lu C-H, Chao Y-C, Hwang S-M, Chen C-L, et al. Simultaneous induction of autophagy and toll-like receptor signaling pathways by graphene oxide. *Biomaterials*. 2012;33(27):6559–69.
27. Chang Y, Yang S-T, Liu J-H, Dong E, Wang Y, Cao A, et al. In vitro toxicity evaluation of graphene oxide on A549 cells. *Toxicol Lett*. 2011;200(3):201–10.
28. Singh SK, Singh MK, Kulkarni PP, Sonkar VK, Grácio JJA, Dash D. Amine-Modified Graphene: Thrombo-Protective Safer Alternative to Graphene Oxide for Biomedical Applications. *ACS Nano*. 2012 Mar 27;6(3):2731–40.
29. Sasidharan A, Panchakarla LS, Chandran P, Menon D, Nair S, Rao CNR, et al. Differential nano-bio interactions and toxicity effects of pristine versus functionalized graphene. *Nanoscale*. 2011;3(6):2461.
30. Mullick Chowdhury S, Lalwani G, Zhang K, Yang JY, Neville K, Sitharaman B. Cell specific cytotoxicity and uptake of graphene nanoribbons. *Biomaterials*. 2013 Jan;34(1):283–93.
31. McIntyre J, Verma NK, Smith RJ, Moore C, Nerl H, McEvoy N, et al. A comparison of catabolic pathways induced in primary macrophages by pristine single walled carbon nanotubes and pristine graphene. *RSC Adv*. 2016;6(70):65299–310.
32. Chng ELK, Pumera M, Novoselov KS, Geim AK, Morozov S, Jiang D, et al. Toxicity of graphene related materials and transition metal dichalcogenides. *RSC Adv*.

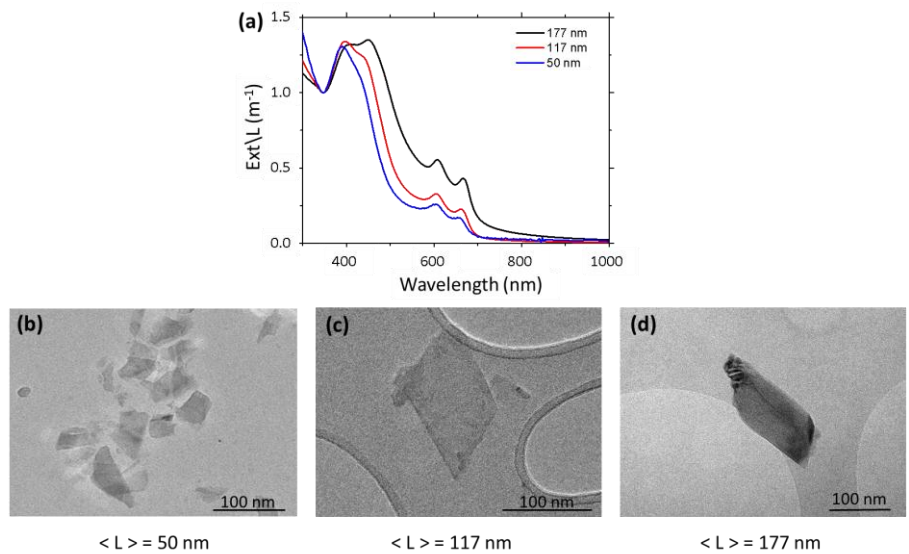
2015;5(4):3074–80.

33. Chng ELK, Sofer Z, Pumera M, Matte H, Gomathi A, Manna AK, et al. MoS<sub>2</sub> exhibits stronger toxicity with increased exfoliation. *Nanoscale*. 2014 Oct 23;6(23):14412–8.
34. Buzea C, Pacheco Blandino II, Robbie K. Nanomaterials and nanoparticles: Sources and toxicity. *Biointerphases*. 2007;2(4):17–172.
35. Kuhlbusch TA, Asbach C, Fissan H, Göhler D, Stintz M. Nanoparticle exposure at nanotechnology workplaces: a review. Part *Fibre Toxicol*. 2011;8:22.
36. Verma NK, Conroy J, Lyons PE, Coleman J, O'Sullivan MP, Kornfeld H, et al. Autophagy induction by silver nanowires: A new aspect in the biocompatibility assessment of nanocomposite thin films. *Toxicol Appl Pharmacol*. 2012;264(3):451–61.
37. Yang Li. Endotoxin contamination: An interference for nanosafety studies | NanoTOES [Internet]. 2014 [cited 2016 Sep 13]. Available from: <http://nanotoes.sbg.ac.at/scientific-challenges/endotoxin-contamination.html>
38. Alexander C, Rietschel ET. Bacterial lipopolysaccharides and innate immunity. *J Endotoxin Res*. 2001;7(3):167–202.
39. Laia SG, Pesudo Q, Totaro S, Sintes JR, Crutzen H. NANoREG harmonised terminology for environmental health and safety assessment of nanomaterials.
40. Khan U, Porwal H, Óneill A, Nawaz K, May P, Coleman JN. Solvent-exfoliated graphene at extremely high concentration. *Langmuir*. 2011;27(15):9077–82.
41. Lutz MB, Kukutsch N, Ogilvie AL., Rößner S, Koch F, Romani N, et al. An advanced culture method for generating large quantities of highly pure dendritic cells from mouse bone marrow. *J Immunol Methods*. 1999;223(1):77–92.
42. Yameen B, Choi W II, Vilos C, Swami A, Shi J, Farokhzad OC. Insight into nanoparticle cellular uptake and intracellular targeting. *J Control Release*. 2014 Sep 28;190:485–99.
43. Jones CF, Grainger DW. In vitro assessments of nanomaterial toxicity. *Adv Drug Deliv Rev*. 2009;61(6):438–56.

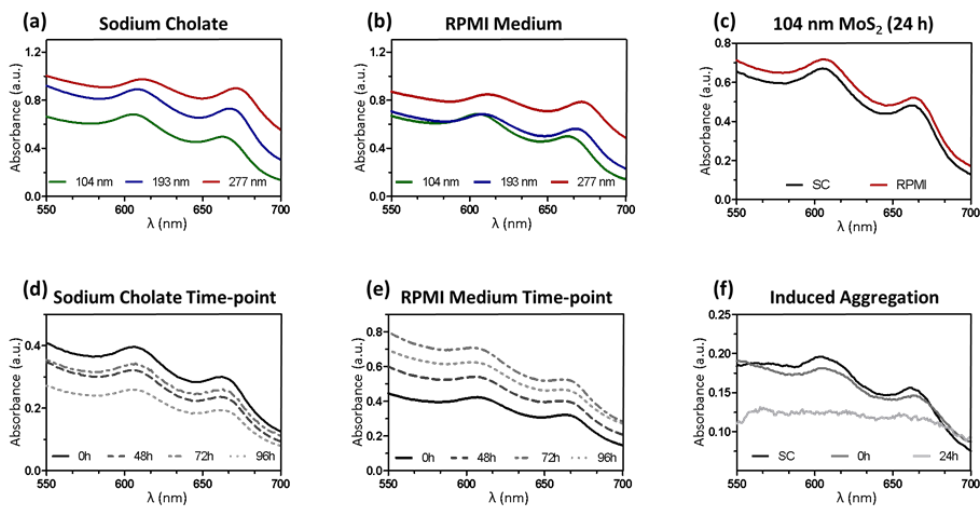


44. Jiang J-W, Kim SY, Park HS. Auxetic nanomaterials: Recent progress and future development. *Appl Phys Rev*. 2016 Dec;3(4):41101.
45. Sur UK, Kumar U. Graphene: A Rising Star on the Horizon of Materials Science. *Int J Electrochem*. 2012;2012:1–12.
46. Ong KJ, MacCormack TJ, Clark RJ, Ede JD, Ortega VA, Felix LC, et al. Widespread nanoparticle-assay interference: implications for nanotoxicity testing. *PLoS One*. 2014;9(3):e90650.
47. Mao P, Wu S, Li J, Fu W, He W, Liu X, et al. Human alveolar epithelial type II cells in primary culture. *Physiol Rep*. 2015 Feb 1;3(2).
48. Gordon S. The macrophage: Past, present and future. *Eur J Immunol*. 2007 Nov;37(S1):S9–17.
49. Golstein P, Kroemer G. Cell death by necrosis: towards a molecular definition. *Trends Biochem Sci*. 2007;32(1):37–43.
50. Elmore S. Apoptosis: a review of programmed cell death. *Toxicol Pathol*. 2007 Jun;35(4):495–516.
51. Shang L, Nienhaus K, Nienhaus GU. Engineered nanoparticles interacting with cells: size matters. *J Nanobiotechnology*. 2014;12(1):5.
52. Slocum C, Coats SR, Hua N, Kramer C, Papadopoulos G, Weinberg EO, et al. Distinct Lipid A Moieties Contribute to Pathogen-Induced Site-Specific Vascular Inflammation. Gunn JS, editor. *PLoS Pathog*. 2014 Jul 10;10(7):e1004215.
53. Vetten MA, Yah CS, Singh T, Gulumian M. Challenges facing sterilization and depyrogenation of nanoparticles: effects on structural stability and biomedical applications. *Nanomedicine*. 2014 Oct;10(7):1391–9.
54. Parameswaran N, Patial S. Tumor necrosis factor- $\alpha$  signaling in macrophages. *Crit Rev Eukaryot Gene Expr*. 2010;20(2):87–103.
55. Oh N, Park J-H. Endocytosis and exocytosis of nanoparticles in mammalian cells. *Int J Nanomedicine*. 2014;9 Suppl 1(Suppl 1):51–63.

**Supplemental Information**

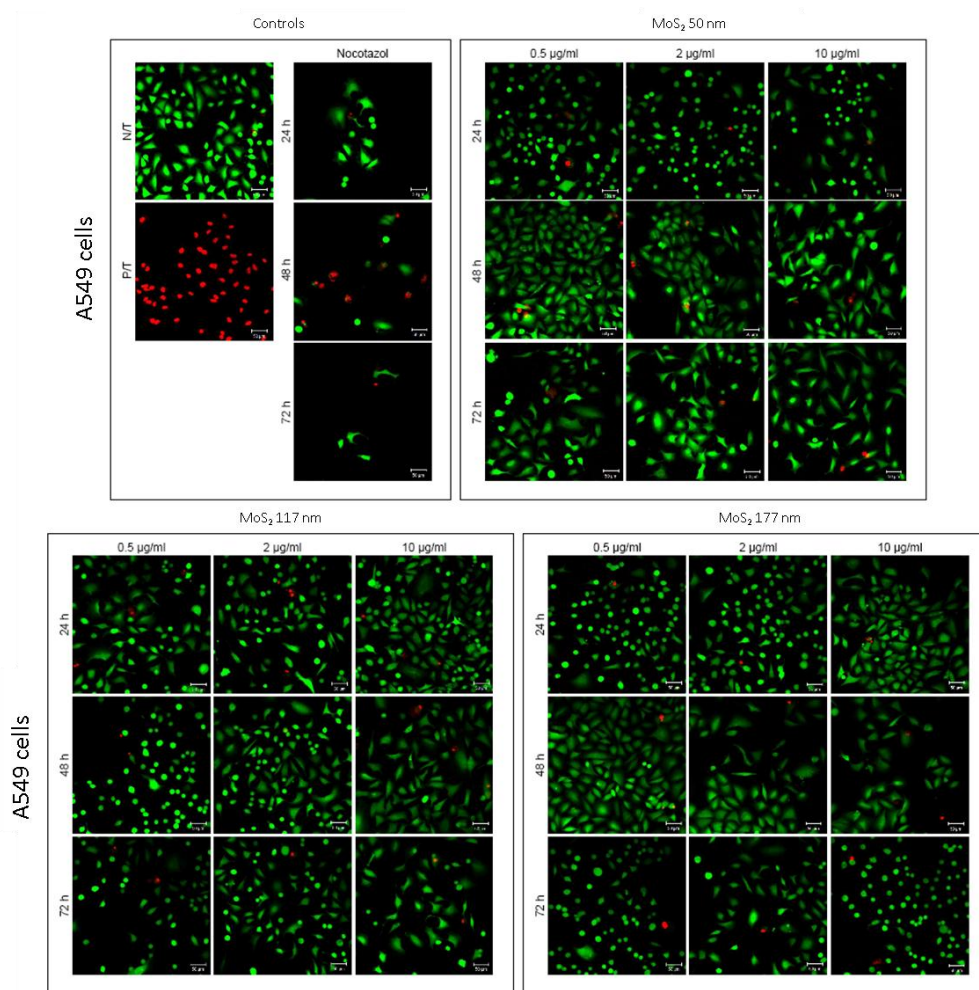


**Supplemental 1:** Material characterization of MoS<sub>2</sub> material: (a) UV-vis spectra of 50 nm (blue), 117 nm (red) and 177 nm (black) nanomaterial. Supplemental figure 1(b) – (d) Transmission electron microscopy images of MoS<sub>2</sub> flakes stabilised in water by sodium cholate. TEM images acquired by JEOL 2100 operated at 200kV.

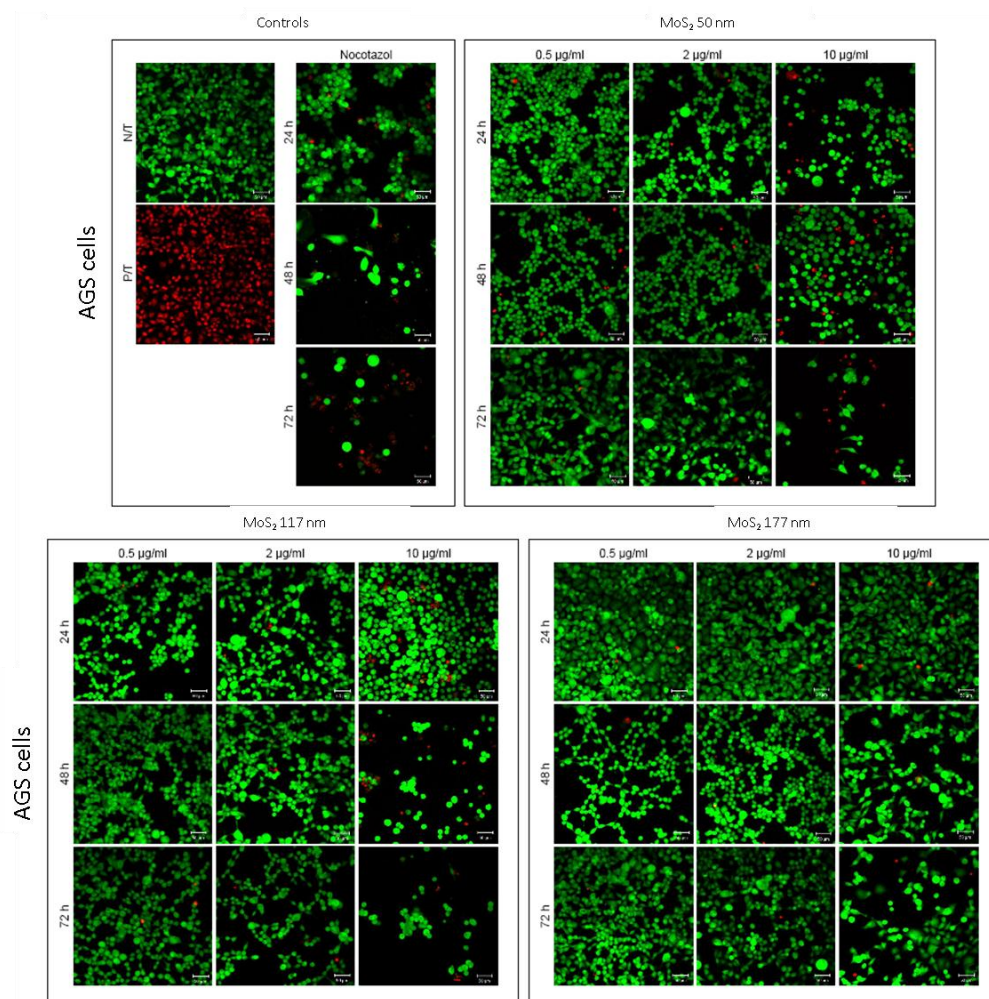


**Supplemental 2:** Representative UV-Vis spectra of MoS<sub>2</sub> material of three sizes following dispersion in surfactant, supplemented cell culture medium and high salt content. Supplemental figure 2(a) dispersion in sodium cholate, 2(b) dispersion in supplemented RPMI, 2(c) 104 nm MoS<sub>2</sub> incubated in SC (black) and RPMI (red) for 24 h, 2(d) 104 nm MoS<sub>2</sub> dispersion in SC and recorded following 0, 48, 72 and 96 h incubation, 2(e) 104 nm MoS<sub>2</sub> dispersed in supplemented RPMI

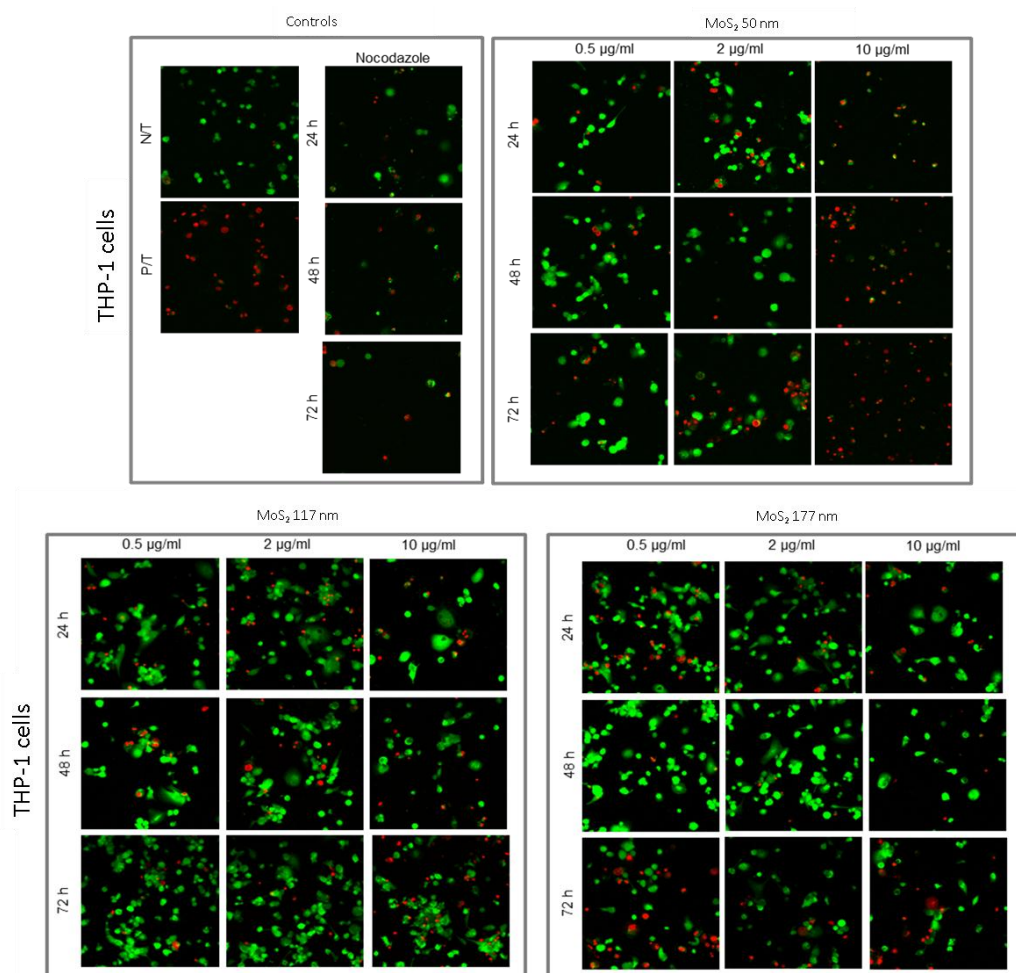
and recorded following 0, 48, 72 and 96 h incubation, 2(f) 104 nm MoS<sub>2</sub> dispersion in sodium chloride (NaCl 40 mg/ml) to induce aggregation and measured following 24 h incubation.



**Supplemental 3a:** Live/Dead viability images of untreated A549 cells following 24, 48 and 72 h exposure to 0.5, 2 and 10 µg/ml of three sizes of MoS<sub>2</sub> nanomaterials (50 nm, 117 nm and 177 nm). Images were acquired on a Zeiss LSM 5 10 confocal microscope under low magnification (x20 objective lens). Green – live cells and red – dead/dying cells. Control samples as indicated N/T – negative control and P/T – positive control.



**Supplemental 3b:** Live/Dead viability images of untreated AGS cells following 24, 48 and 72 h exposure to 0.5, 2 and 10 μg/ml of three sizes of MoS<sub>2</sub> nanomaterials (50 nm, 117 nm and 177 nm). Images were acquired on a Zeiss LSM 5 10 confocal microscope under low magnification (x20 objective lens). Green – live cells and red – dead/dying cells. Control samples as indicated N/T – negative control and P/T – positive control.



**Supplemental 3c:** Live/Dead viability images of untreated THP-1 cells following 24, 48 and 72 h exposure to 0.5, 2 and 10 μg/ml of three sizes of MoS<sub>2</sub> nanomaterials (50 nm, 117 nm and 177 nm). Images were acquired on a Zeiss LSM 5 10 confocal microscope under low magnification (x20 objective lens). Green – live cells and red – dead/dying cells. Control samples as indicated N/T – negative control and P/T – positive control.

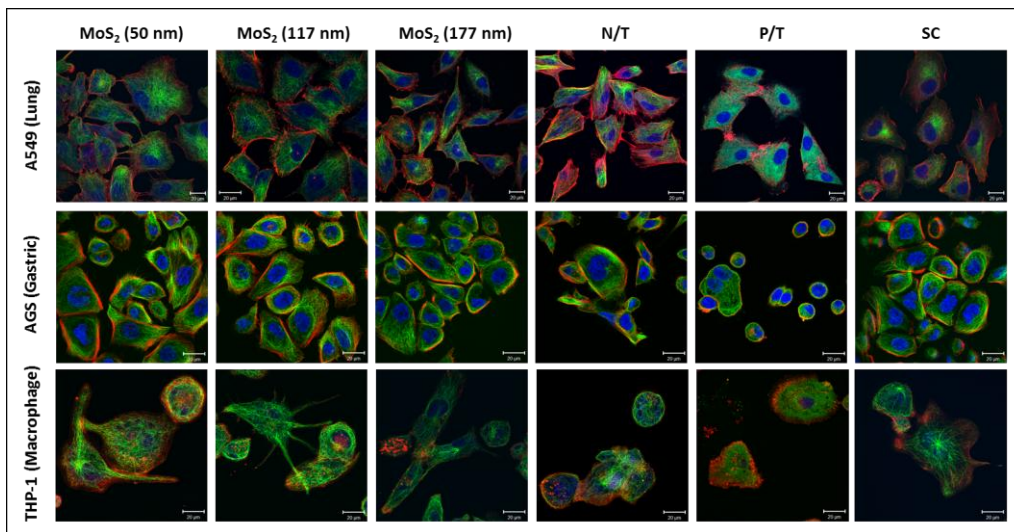
Size	Concentration (μg/ml)	Time	A549	AGS	THP-1
------	-----------------------	------	------	-----	-------

		N/T	100.00	100.00	100.00
		P/T	0.00	0.00	2.41
50 nm	0.5	24h	98.59	99.73	92.29
		48h	96.92	98.78	96.29
		72h	99.52	99.54	96.04
	2	24h	99.67	99.78	87.44
		48h	96.77	99.37	99.99
		72h	99.37	99.60	77.35
	10	24h	99.84	95.76	64.60
		48h	99.62	95.89	35.28
		72h	96.90	93.40	14.11

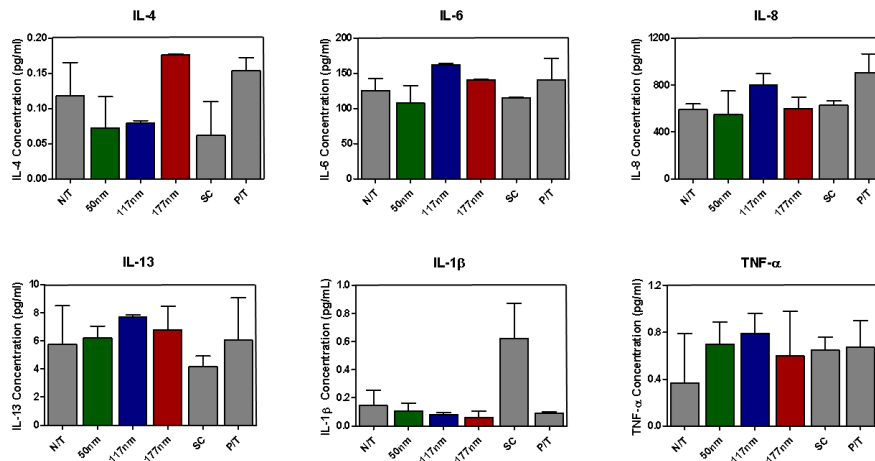
Size	Concentration (µg/ml)	Time	A549	AGS	THP-1
		N/T	100.00	100.00	100.00
		P/T	0.00	0.00	2.41
117 nm	0.5	24h	99.02	99.85	97.06
		48h	99.75	100.01	92.42
		72h	98.31	99.48	98.44
	2	24h	98.35	99.54	95.76
		48h	100.11	99.74	96.01
		72h	99.72	99.58	100.61
	10	24h	99.79	97.45	92.92
		48h	98.11	92.95	95.03
		72h	99.03	97.63	88.43

Size	Concentration (µg/ml)	Time	A549	AGS	THP-1
		N/T	100.00	100.00	100.00
		P/T	0.00	0.00	2.41
177 nm	0.5	24h	99.51	99.81	89.28
		48h	98.03	99.57	101.21
		72h	98.12	99.92	70.08
	2	24h	99.84	99.89	97.83
		48h	99.41	99.63	102.09
		72h	98.49	99.91	90.56
	10	24h	96.83	99.11	94.33
		48h	98.30	99.77	99.57
		72h	98.78	99.49	75.50

**Supplemental 3d:** Live/Dead viability table of untreated A549, AGS and THP-1 cells following exposure to 24, 48 and 72 h exposure to 0.5, 2 and 10 µg/ml of three sizes of MoS<sub>2</sub> nanomaterials (50 nm, 117 nm and 177 nm). Control samples as indicated N/T – negative control and P/T – positive control. Cell viability percentage has been normalized to negative controls for each cell line. Cell viability as quantified by Image J.

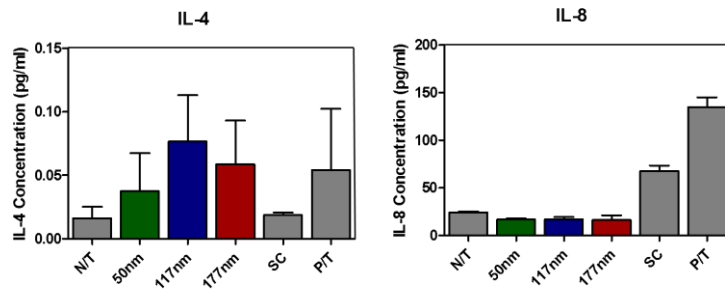


**Supplemental 4:** Confocal microscopic images of untreated THP-1, AGS and A549 cells and following 4 h exposure to 1 µg/ml of three different MoS<sub>2</sub> nanomaterial sizes (50 nm, 117 nm and 177 nm). Images were acquired on a Zeiss LSM 5 10 confocal microscope under oil immersion (63x magnification). Red – F-actin, green – α-tubulin and blue –nucleus. N/T – negative treatment control, P/T – positive treatment, SC – sodium cholate (scale bars: 20µm).

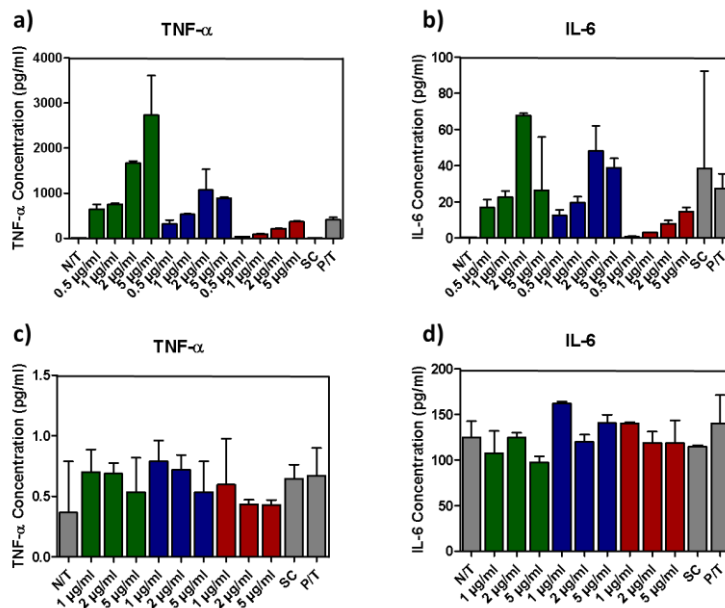


**Supplemental 5A:** IL-4, IL-6, IL-8, IL-13, TNF-α and IL-1β cytokine responses of A549 cells as determined by MSD multi-plex 10-spot inflammatory ELISA kit. Cytokine response shown is recorded from supernatants of A549 cells following 24 h exposure to 1 µg/ml of MoS<sub>2</sub> nanomaterial (50 nm, 117 nm and 177 nm). Green – 50 nm, blue – 117 nm, red – 177 nm, grey – controls (N/T – not treated, SC – sodium cholate, P/T – positive treatment).





**Supplemental 5B:** IL-4 and IL-8 cytokine responses of AGS cells as determined by MSD multi-plex 10-spot inflammatory ELISA kit. Cytokine response shown is recorded from supernatants of AGS cells following 24 h exposure to 1  $\mu\text{g/ml}$  of  $\text{MoS}_2$  nanomaterial (50 nm, 117 nm and 177 nm). Green – 50 nm, blue – 117 nm, red – 177 nm, grey – controls (N/T – not treated, SC – sodium cholate, P/T – positive treatment).



**Supplemental 5C:** TNF- $\alpha$  and IL-6 cytokine responses of THP-1 and A549 cells as determined by MSD multi-plex 10-spot inflammatory ELISA kit. Cytokine response shown is recorded from supernatants of cells following 24 h exposure to a range of concentrations (1, 2 and 5  $\mu\text{g/ml}$ ) of  $\text{MoS}_2$  nanomaterial (50 nm, 117 nm and 177 nm). A-B: THP-1 cell response, C-D: A549 cell response. Green – 50 nm, blue – 117 nm, red – 177 nm, grey – controls (N/T – Not treated, SC – Sodium Cholate, P/T – positive treatment).